SUPPLEMENTARY MATERIALS AND METHODS

Confocal microscopy, immunohistochemistry and quantification of synaptic parameters

Larvae were dissected in low Ca^{2+} HL3.1 solution of composition (in mM): 70 NaCl, 5 KCl, 0.2 $CaCl_2$, 20 $MgCl_2$, 10 $NaHCO_3$, 5 Trehalose, 115 Sucrose, 5 HEPES, pH 7.2. Dissected NMJ preparations were fixed in either 4% PFA (in PBS) or Bouin's solution for 10-20 mins at room temperature. Antibodies were diluted in PBS with 0.15% Triton-X and 5% goat serum. The following antibodies were used for larval and adult immunostaining: mouse anti-BRP (nc82, 1:200), anti-CSP (6D6-c, 1:1000), anti-FASII (1D4-c, 1:400) and anti-Futsch (22C10, 1:200) (Developmental Studies Hybridoma Bank); rabbit anti-GFP (1:1000) (Invitrogen); rabbit anti-GLURIIC (1:5000, kind gift of Aaron DiAntonio). Fluorescence conjugated secondary antibodies and anti-HRP were obtained from Molecular Probes (Invitrogen) and Jackson ImmunoResearch, respectively. For quantification of synaptic bouton number, all experiments were performed and analyzed blind to experimental genotype. Boutons were identified using anti-HRP and anti-CSP (Zinsmaier et al., 1990). Both type 1b and type 1s boutons were included in the bouton count. Synaptic bouton and AZ areas were quantified using ImageJ. Since small boutons were difficult to accurately measure, we set a minimum cut-off point of 5 μm^2 for all genotypes. The number of BRP puncta was quantified using the ImageJ 3D Object Counter plug-in, using a constant threshold.

Reverse Transcriptase (RT) PCR

Fly head mRNA was extracted using TRIzol (Life Technologies), and reverse transcribed using High Capacity cDNA Reverse Transcriptase Kit (Applied Biosystems). RT-PCR was performed using the following primers: 5'-ATA CCA TGG AGT ACG GGG GC-3' and 5'-ATA AGC TTC CGT CAC TAG CGT GTG C-3' for *dysc*; 5'-GCC GAT GAT TGT CTC AAG GT-3' and 5'-GAT ACG AAG GAC GGG GGT AT-3' for *slo*; and 5'-CGG AAT TCC GGC AAG ATG TGG ACG C-3' and 5'-AAC TCG AGC TAT CTG CTG AGC AAT TGA CC-3' for *sleepless* (*sss)*, which was used as a positive control.

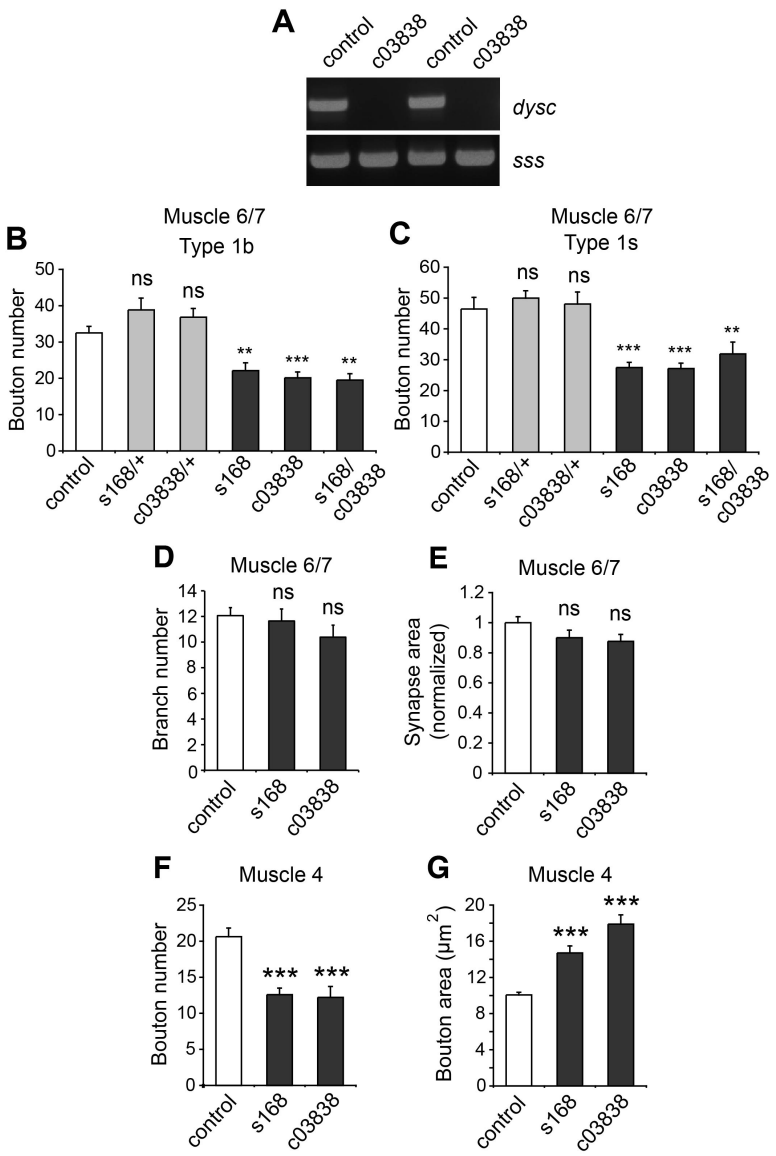

Fig. S1. Alterations in larval synaptic morphology in *dysc* mutants. (A) Two independent RT-PCR reactions from wild type control and *dysc*^{c03838} head cDNA using primers flanking the c03838 insertion site. No wild-type *dysc* mRNA expression was detected in *dysc*^{c03838} homozygotes. RT-PCR of *sleepless* (*sss*) mRNA expression was used as a control. (B-C) Average number of type 1b (B) and type 1s (C) synaptic boutons at muscle 6/7, segment 3, in wild type controls, *dysc*^{s168} and *dysc*^{c03838} heterozygotes and homozygotes, and *dysc*$^{c03838/s168}$ trans-heterozygotes. n = 12-29 synapses. (D) Average number of synaptic branches at muscle 6/7, segment 3, in control, *dysc*^{s168} and *dysc*^{c03838} larvae. n = 13-16. (E) Average synaptic area at muscle 6/7, segment 3, in control, *dysc*^{s168} and *dysc*^{c03838} larvae. Synaptic area was normalized to the muscle 6/7 area for each synapse. n = 20-23. (F-G) Average bouton number (F) and size (G) at muscle 4, segment 3, in control, *dysc*^{s168} and *dysc*^{c03838} larvae. F: n = 15-19 synapses. G: n = 96-176 boutons. Values represent mean ± s.e.m. ** $P < 0.005$, *** $P < 0.0005$; ns – $P > 0.05$, one-way ANOVA with Dunnett post-hoc test.

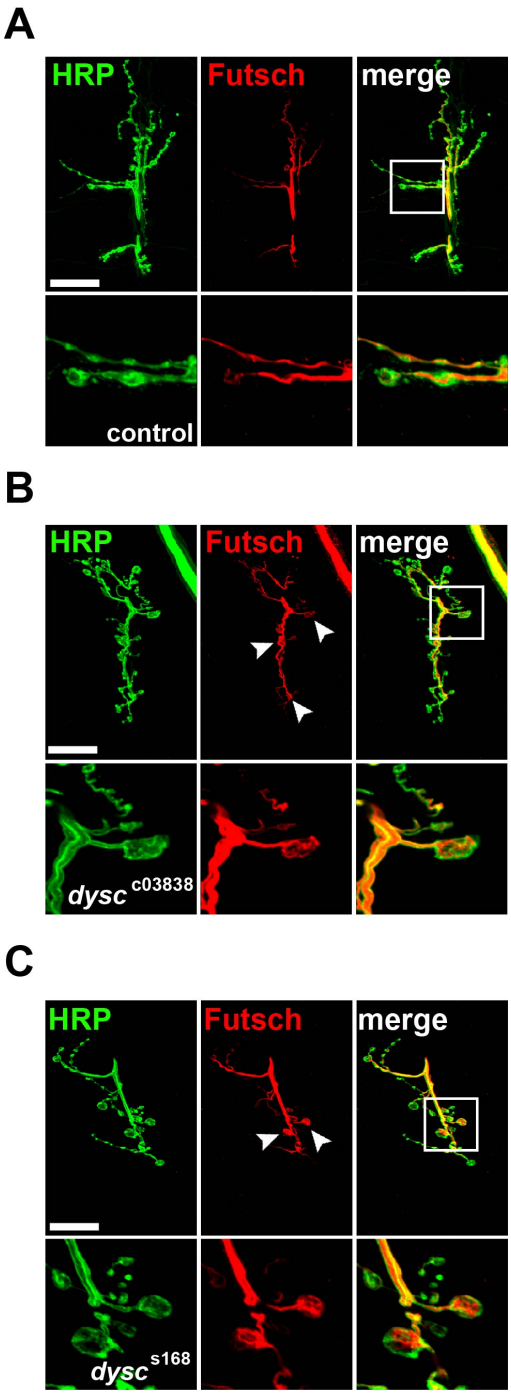

Fig. S2. Futsch mis-localization in *dysc* mutant synapses. (A-C) Representative confocal z-stacks of HRP-labeled synapses at muscle 6/7 co-stained with anti-Futsch antibodies in wild type control (A), *dysc*^{s168} (B) and *dysc*^{c03838} (C) larvae. Upper panels show images of the complete synapse. No clear alteration of Futsch localization was observed in the axonal regions in either *dysc* mutant background. Arrows point to synaptic boutons exhibiting abnormal Futsch localization, examples of which are shown in magnified images below. Scale bars, 20 μm.

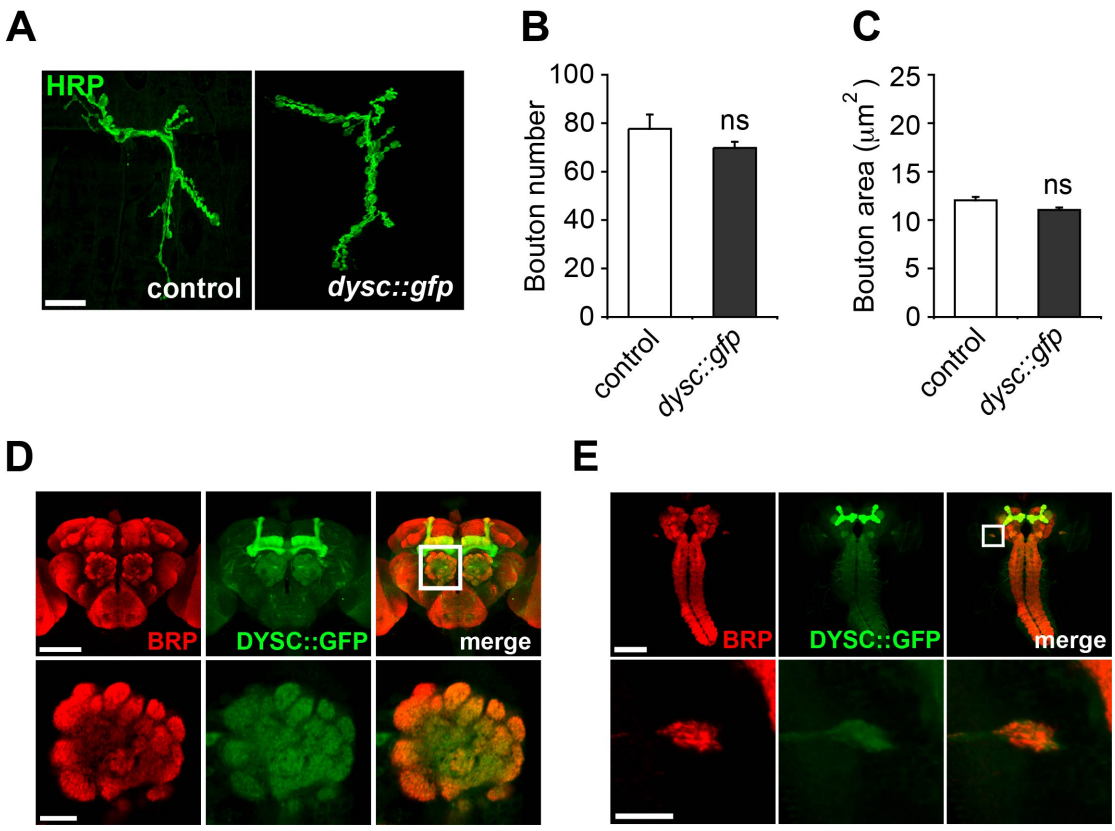

Fig. S3. DYSC::GFP expression in the adult and larval nervous systems. (A) Representative confocal images of HRP-labeled synapses in wild type control and *dysc::gfp* homozygous larvae. Scale bar, 20 μm. (B-C) Bouton number (B) and size (C) were unchanged in *dysc::gfp* homozygotes. *n*-values: (B) – control: $n = 15$, *dysc::gfp*: $n = 19$; (C) – control: $n = 296$, *dysc::gfp*: $n = 339$. Values represent mean ± s.e.m. ns – $P > 0.05$, Mann-Whitney U-test. (D-E) DYSC::GFP expression in the adult (D) and larval (E) brain, visualized using an anti-GFP antibody. Brains were counterstained with anti-Bruchpilot (BRP) to image synaptic neuropil regions. Enlarged images of the adult antennal lobe (D, lower panels) and a synaptic region projecting to the lateral region of the larval brain (E, lower panels) are shown. Scale bars: upper panels – 100 μm, lower panels – 20 μm.

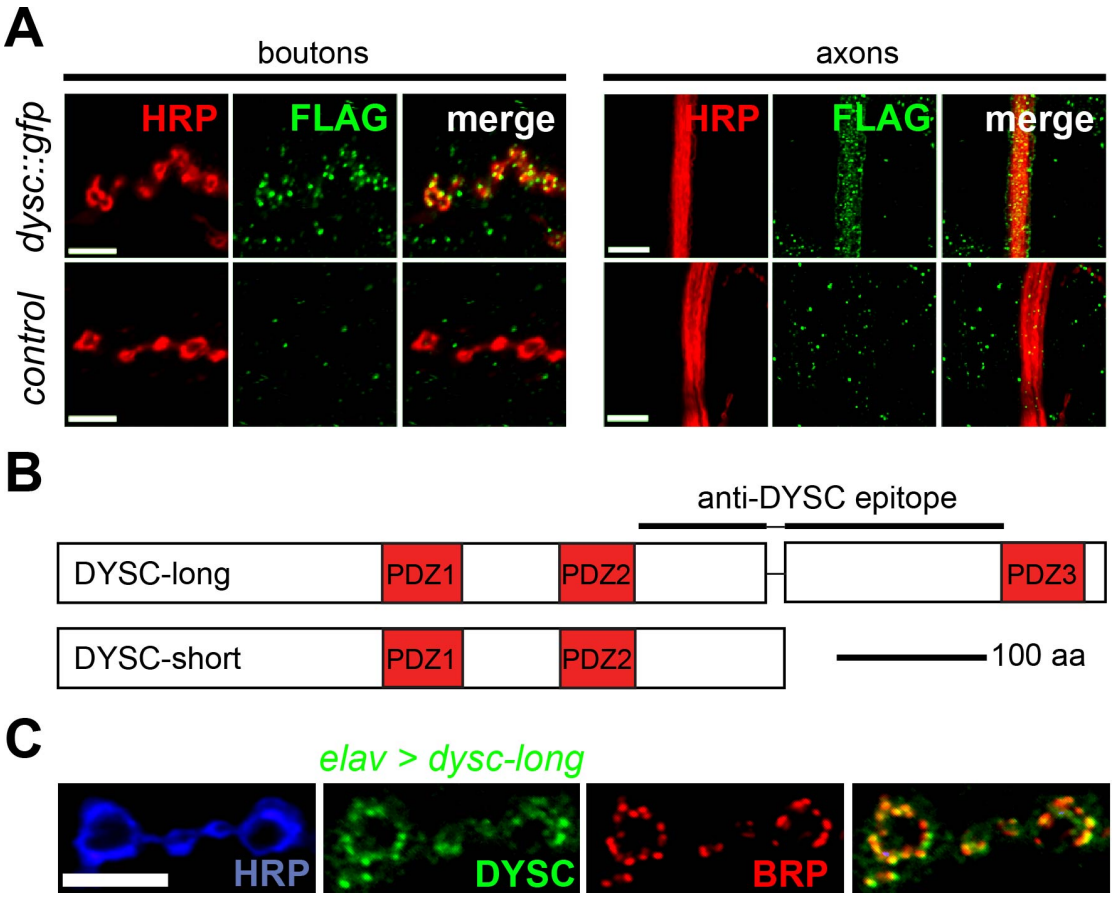

Fig. S4. DSYC::GFP and over-expressed wild-type DYSC exhibit similar patterns of localization. (A) Antibodies to an independent segment of the protein trap (3xFLAG), yielded a similar punctate localization to that observed when using anti-GFP (Fig. 2A) in both larval motor neuron synaptic boutons and axon bundles labeled using anti-HRP. This expression pattern was not detected in controls lacking the *dysc::gfp* allele. Scale bars: boutons – 10 μm, axons – 5 μm. (B) Schematic of the DYSC protein isoforms illustrating the antigen used to generate the anti-DYSC antibody (Jepson et al., 2012) Isoform C, one of the long isoforms (www.flybase.org), was used as a template to generate the antigen. (C) Neuronal over-expression of a long DYSC transgene using *elav*-Gal4 and immunostained with anti-DYSC recapitulates the punctate expression pattern seen using anti-GFP and anti-FLAG in *dysc::gfp* homozygotes. DYSC puncta closely co-localized with the active zone marker BRP, as demonstrated for DYSC::GFP in Fig. 3A. Scale bar, 5 μm.

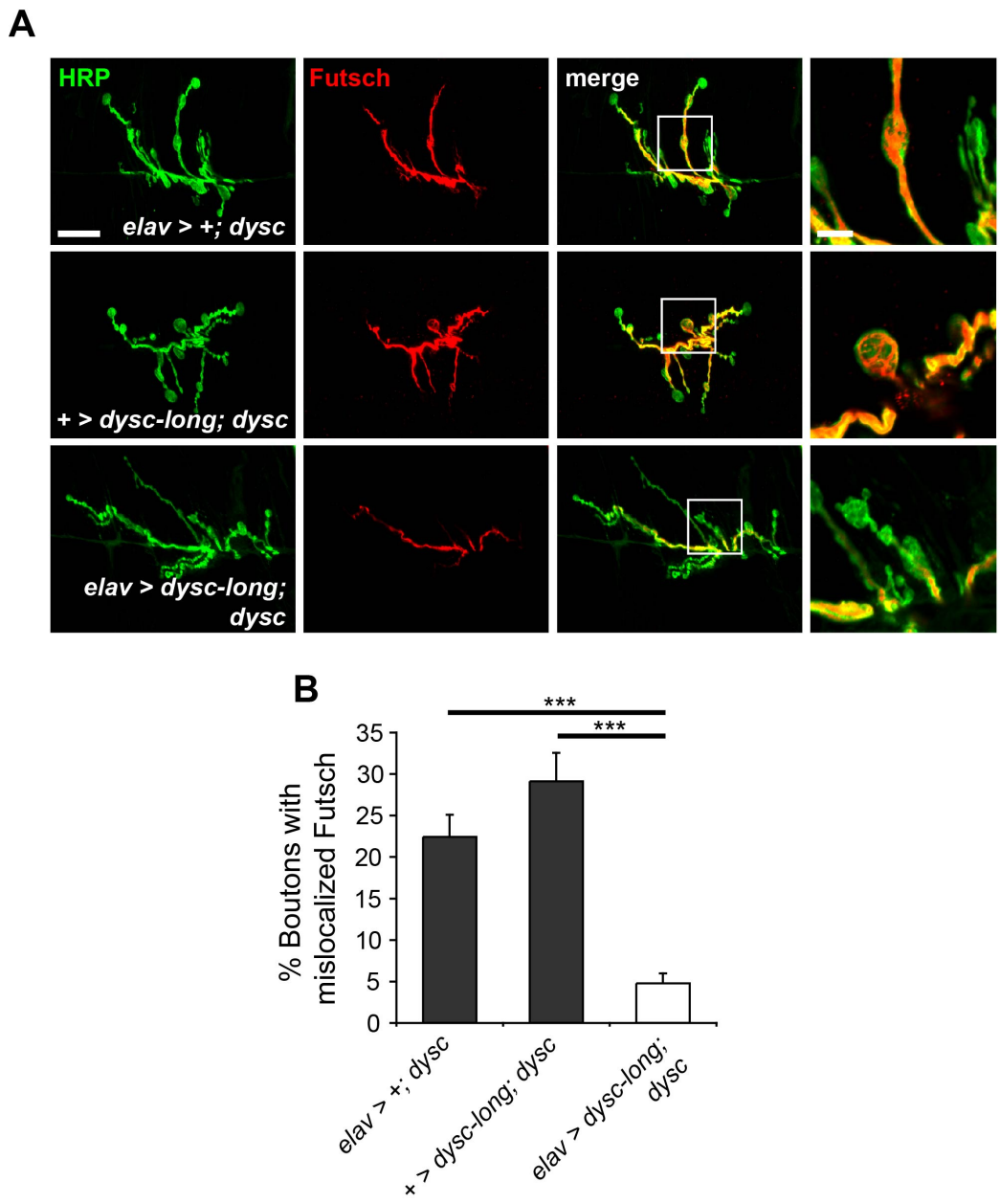

Fig. S5. Presynaptic expression of DYSC rescues Futsch mis-localization in *dysc* mutants. (A) Representative confocal z-stacks of HRP- and Futsch-labeled synapses in *dysc*^{c03838} (*dysc*) mutants harboring either the pan-neuronal *elav*-Gal4 (*elav*) driver, a *uas-dysc-long* transgene (*dysc-long*) or both. Areas within boxes are magnified in the right panels. Note the extensive Futsch labeling of synapses in *dysc* mutants carrying either the pan-neuronal driver or *uas-dysc-long* transgene alone, but not following presynaptic restoration of DYSC expression. Scale bars: whole synapses – 20 µm, magnified images – 5 µm. (B) Average proportion of boutons exhibiting unbundled Futsch in synaptic boutons. n = 10-12 synapses, 239-337 boutons. Values represent mean ± s.e.m. *** $P <$ 0.0005, one-way ANOVA with Dunnett post-hoc test.

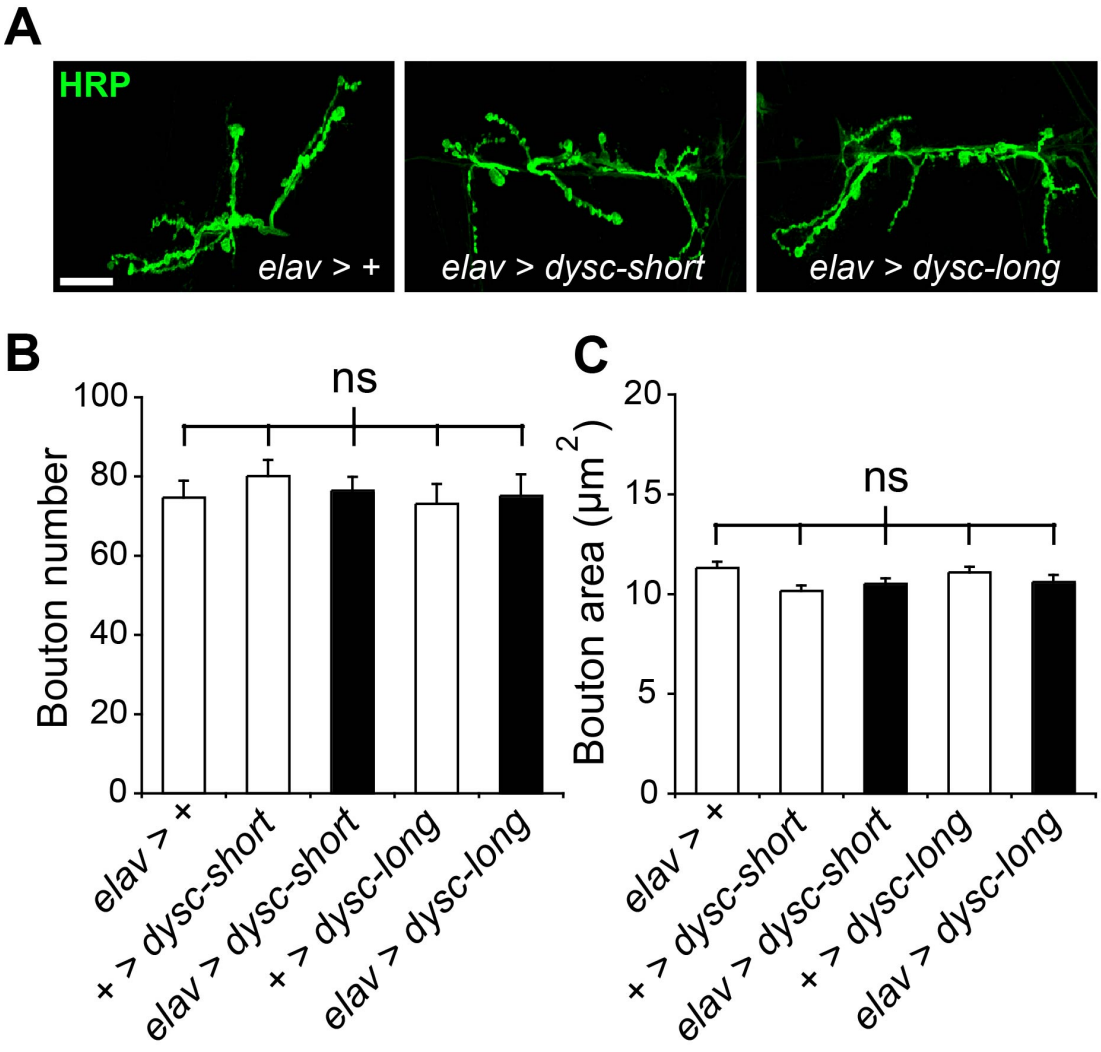

Fig. S6. Overexpression of either long of short DYSC isoforms does not alter synaptic development. (A) Representative confocal projections of control larvae carrying the neuronal *elav*-Gal4 driver (*elav* > +) and larvae over-expressing DYSC isoforms containing either two (*dysc-short*) or three (*dysc-long*) PDZ domains in motor neurons. Scale bar, 20 µm. (B-C) Average bouton number (B: n = 13-23 synapses) and area (C: n = 213-296 boutons) in control genotypes carrying driver or transgenes alone as well as larvae over-expressing DYSC-short or DYSC-long isoforms under control of *elav*-Gal4. Values represent mean ± s.e.m. ns: $P > 0.05$, one-way ANOVA with Tukey's post-hoc test.

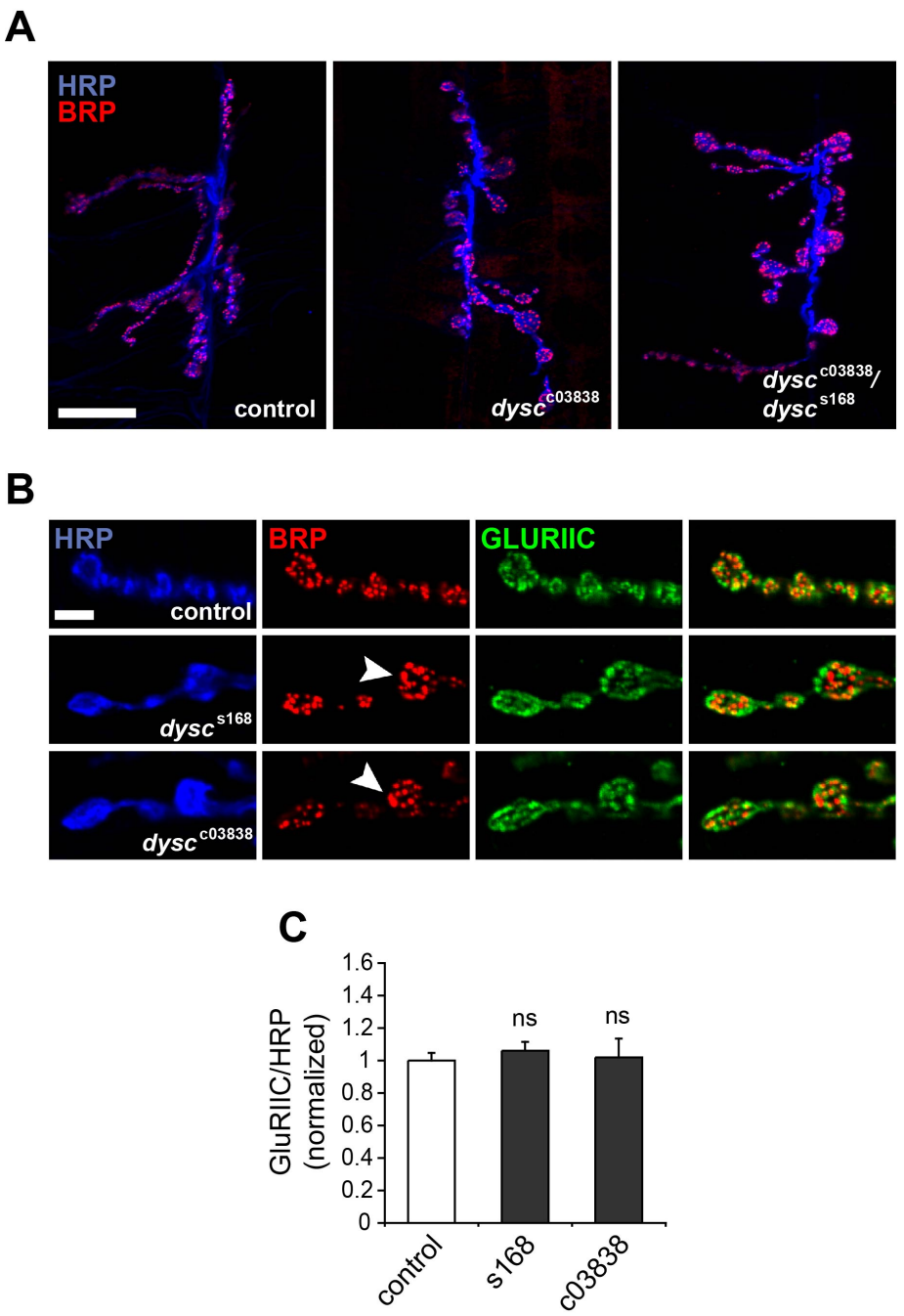

Fig. S7. Normal BRP localization and GLURIIC expression in *dysc* mutants. (A) Confocal projections showing expression and localization of BRP in HRP-labeled wild type and *dysc* synapses. Scale bar, 20 μm. (B) Representative confocal slices illustrating expression of BRP and postsynaptic GLURIIC expression in control larvae and two *dysc* allelic backgrounds are shown. Arrows point to large BRP puncta that were rarely observed in control synapses. Scale bar, 5 μm. (C) Average GLURIIC expression in synaptic boutons from wild type control, *dysc*^{s168} and *dysc*^{c03838} larvae. Fluorescence intensity is normalized to controls. n = 43-55 boutons. Values represent mean ± s.e.m. ns: $P > 0.05$, one-way ANOVA with Dunnett post-hoc test.

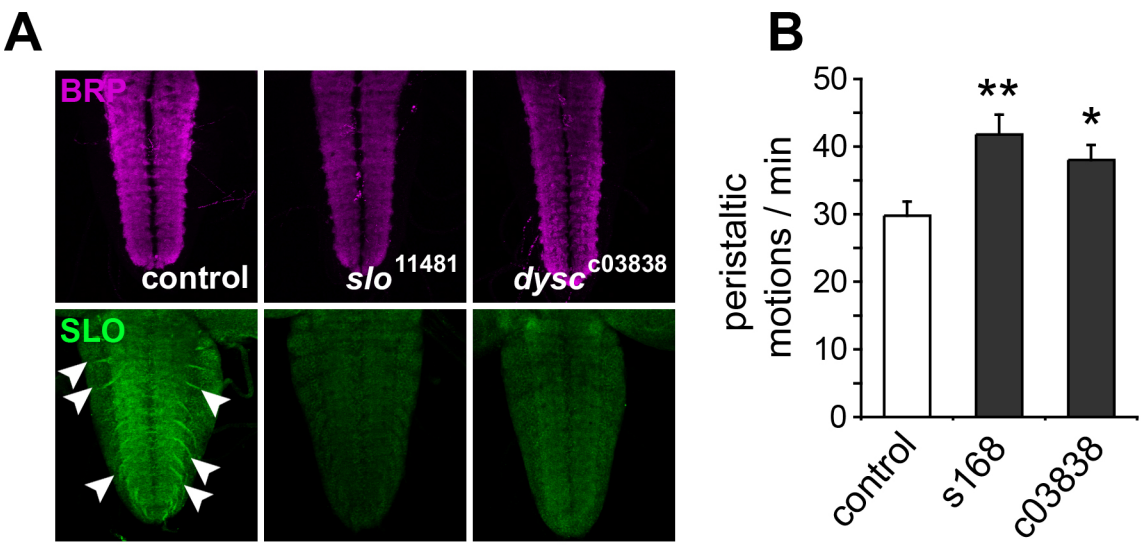

Fig. S8. DYSC regulates SLO expression in the larval nervous system. (A) Confocal z-stacks of ventral nerve cords (VNCs) from control, *slo*^{11481} and *dysc*^{c03838} larvae immuno-stained with anti-Bruchpilot (BRP) and anti-SLO. Arrows point to robust anti-SLO staining in motor neuron axons projecting from the VNC in control, but not *slo*^{11481} and *dysc*^{c03838} larvae. (B) Frequency of larval body wall peristalsis per min during locomotion in wild type controls and two independent *dysc* mutants (*dysc*^{s168} and *dysc*^{c03838}). n = 23-29. Values represent mean ± s.e.m. * $P < 0.05$; ** $P < 0.005$, one-way ANOVA with Dunnett post-hoc test.

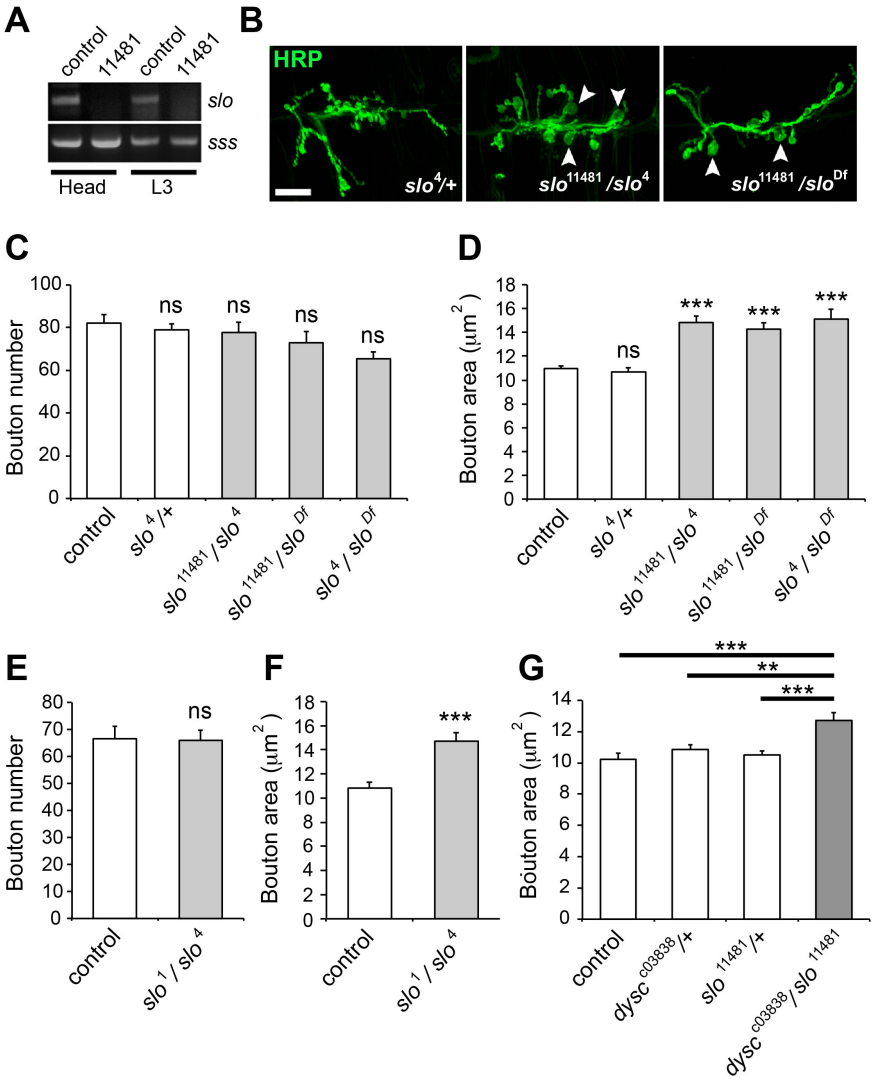

Fig. S9. SLO channels regulate synaptic bouton size. (A) Amplification of *slo* transcripts via RT-PCR from wild type and slo^{11481} adult head or whole 3rd instar (L3) larvae cDNA. *sleepless* (*sss*) mRNA expression was used as a control. (B) Confocal projections of synapses from transheterozygotic combinations of two *slo* null alleles (slo^{4} and slo^{11481}) and a deficiency that removes the *slo* locus (slo^{Df}), as well as slo^{4} heterozygotes. Arrows point to enlarged boutons. Scale bar, 20 μm. (C-D) Average bouton number (C) and bouton area (D) in the above genotypes. n = 9-32 synapses and 133-443 boutons. Note that the same control values are also used in Fig. 4B, C. Values represent mean ± s.e.m. *** $P < 0.0005$; ns – $P > 0.05$, one-way ANOVA with Dunnett post-hoc test. (E-F) Average bouton number (E) and bouton area (F) in control (n = 11 synapses, 113 boutons) and slo^{1}/slo^{4} transgeterozygote larval synapses (n = 15 synapses, 161 boutons). *** $P < 0.0005$, ns – $P > 0.05$, Mann-Whitney U-test. (G) Average synaptic bouton size in wild type controls compared to heterozygotic and transheterozygotic combinations of the $dysc^{c03838}$ and slo^{11481} alleles. n = 150-202 boutons. ** $P < 0.005$, *** $P < 0.0005$, one-way ANOVA with Tukey's post-hoc test. All data were derived from synapses at muscle 6/7, segment 3. Values represent mean ± s.e.m.

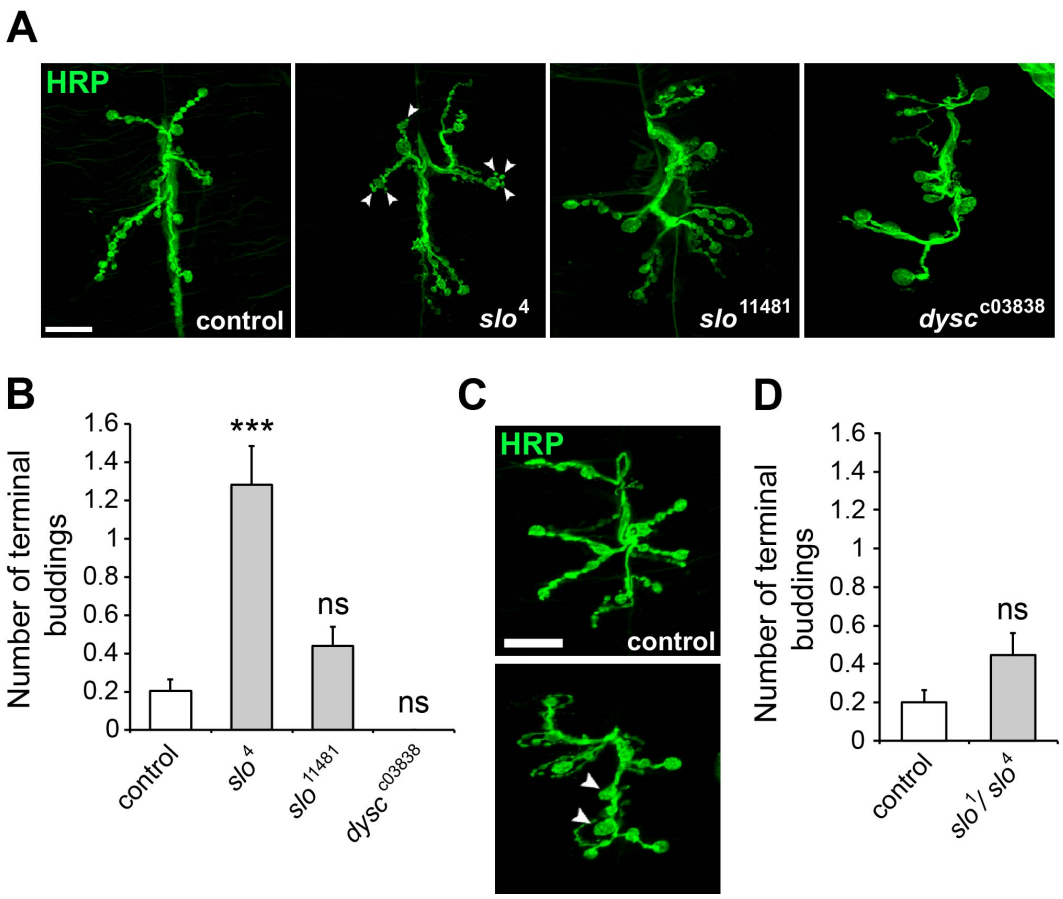

Fig. S10. Homozygosity for the *slo*^{4} inversion results in temperature-sensitive hyper-budding of synaptic boutons. (A) Representative confocal z-stacks of synapses from muscle 6/7, segment 3, from control larvae and *slo*^{4}, *slo*^{11481} and *dysc*^{c03838} homozygotes raised at 18°C. Scale bar, 20 μm. Arrows point to multiple budding events in type 1b boutons of *slo*^{4} homozygotes, a phenotype rarely observed in controls, *slo*^{11481} or *dysc*^{c03838} homozygotes raised at 18°C. (B) Mean number of terminal budding events in type 1b boutons from the above genotypes. n = 12-14 synapses, 59-82 boutons per genotype. (C) Representative confocal z-stacks of synapses from control and *slo*^{1}/*slo*^{4} larvae raised at 18°C. Arrows point to enlarged synaptic boutons. (D) No significant hyper-budding of terminal boutons was observed in this genetic background at 18°C. Thus, the temperature-sensitive hyper-budding of *slo*^{4} homozygotes appears to require two copies of the *slo*^{4} inversion in an iso31 background. Values represent mean ± s.e.m. ns – $P > 0.05$, *** $P < 0.0005$, one-way ANOVA with Dunnett post-hoc test (B) or Mann-Whitney U-test (D).

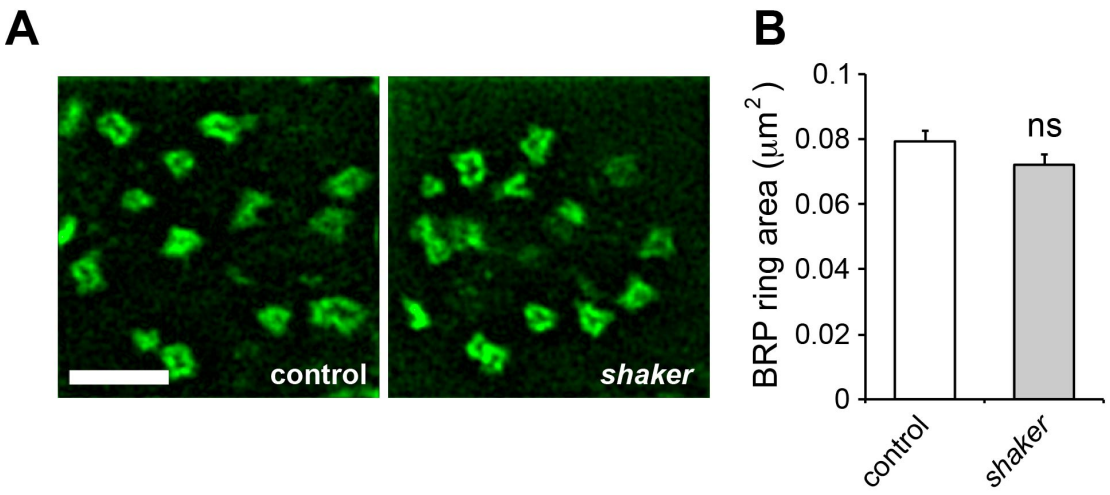

Fig. S11. Loss of the Shaker potassium channel does not impact AZ size or organization. (A) Representative STED images of BRP-labeled AZs in wild type controls and sh^{Df} (*shaker*) mutants, which harbor a small deficiency that specifically removes the *shaker* locus. Scale bar, 1 μm. (B) Average area of individual BRP-labeled AZs in controls and sh^{Df} synapses. In contrast to *slo* mutants (Fig. 5), no increase in the mean area of AZs was observed following loss of *shaker*, and there was no apparent merging of neighboring AZs. Values represent mean ± s.e.m. Control: $n = 51$ AZs, sh^{Df}: $n = 49$. ns – $P > 0.05$, Mann-Whitney U-test.

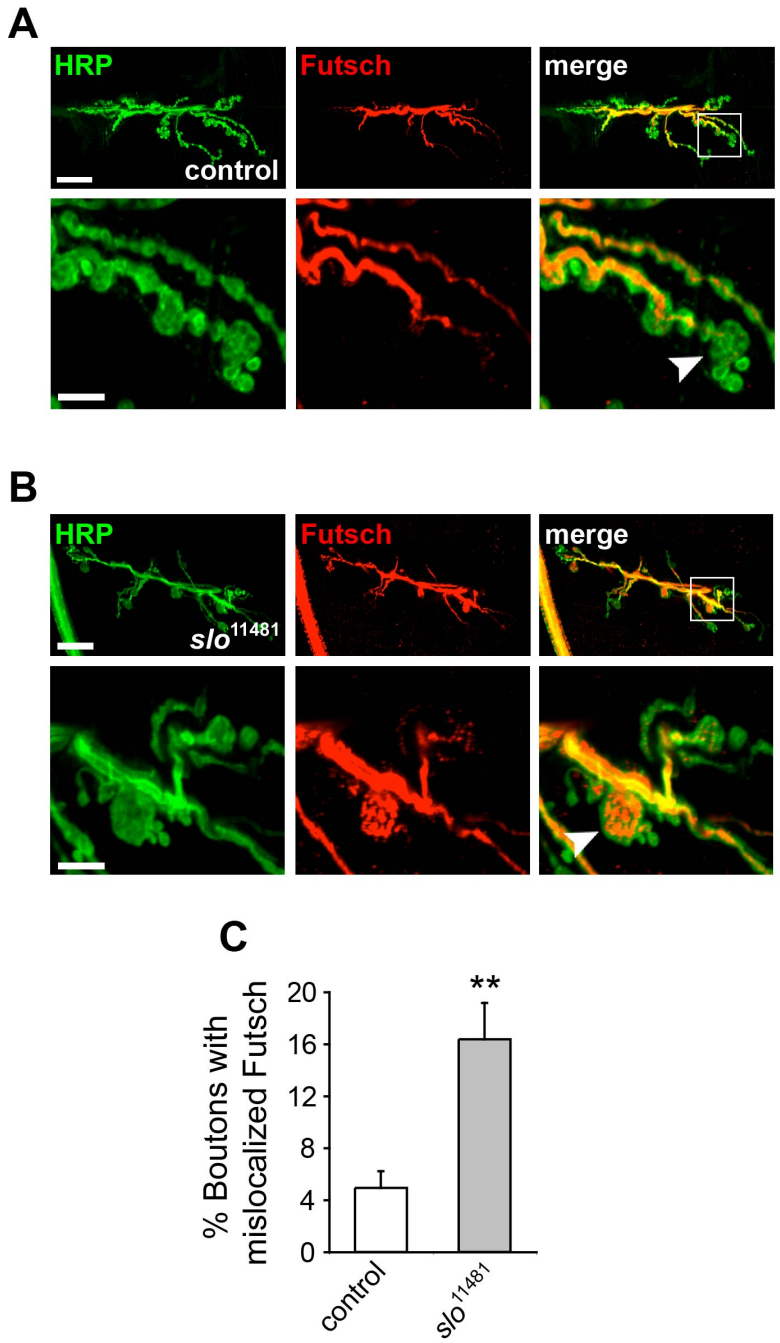

Fig. S12. SLO channels impact the synaptic organization of Futsch. (A, B) Representative confocal z-stacks of synapses at muscle 6/7 from wild type control (A) and *slo*^{11481} (B) larvae labeled with anti-HRP and anti-Futsch antibodies. Magnified panels on the right illustrate synaptic Futsch innervation in the above genetic backgrounds. In *slo*^{11481} synapses, Futsch is often observed in an unbundled, disorganized state, while this is rarely observed in wild type synaptic boutons. Scale bar, 20 μm. (C) Mean proportion of boutons within a given synapse exhibiting unbundled Futsch. Control – n = 15 synapses, 661 boutons; *slo*^{11481} – n = 19 synapses, 554 boutons. Values represent mean ± s.e.m. ** $P < 0.005$, Mann-Whitney U-test.

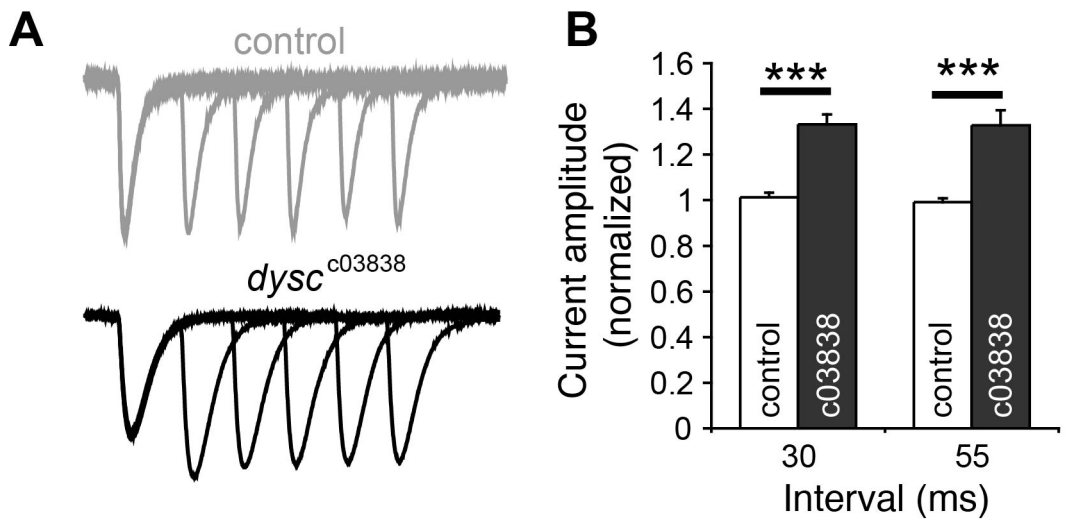

Fig. S13. DYSC modulates short-term synaptic plasticity. (A) Overlaid paired-pulse EJC recordings from control and *dysc*^{c03838} homozygotes. Pairs of EJCs were evoked with an interval of 30 ms (second EJC) or an additional multiple of 25 ms (successive EJCs). Traces were normalized to illustrate changes in paired-pulse facilitation. Note the sustained increase in the EJC currents in *dysc*^{c03838} larvae that are absent in controls. (B) Quantification of paired-pulse facilitation using EJC peaks evoked 30 ms or 55 ms after the initial EJC. Values are normalized to the initial EJC for each genotype. Control – n = 12; *dysc*^{c03838} – n = 9. Values represent mean ± s.e.m. *** $P < 0.0005$, Mann-Whitney U-test.

SUPPLEMENTARY REFERENCES

Jepson, J. E., Shahidullah, M., Lamaze, A., Peterson, D., Pan, H. and Koh, K. (2012). *dyschronic*, a *Drosophila* homolog of a deaf-blindness gene, regulates circadian output and Slowpoke channels. *PLoS Genetic* **8**, e1002671.

Zinsmaier, K. E., Hofbauer, A., Heimbeck, G., Pflugfelder, G. O., Buchner, S. and Buchner, E. (1990). A cysteine-string protein is expressed in retina and brain of *Drosophila*. *J Neurogenet* **7**, 15-29.